High Critical-Current Density in the Heavily Pb-Doped $Bi_2Sr_2CaCu_2O_{8+\delta}$ Superconductor: Generation of Efficient Pinning Centers

I. Chong, Z. Hiroi,* M. Izumi, J. Shimoyama, Y. Nakayama, K. Kishio, T. Terashima, Y. Bando, M. Takano

Critical-current density (J_c) is a parameter of primary importance for potential applications of high-temperature copper oxide superconductors. It is limited principally by the breakdown of zero-resistive current due to thermally activated flux flow at high temperatures and high magnetic fields. One promising method to overcome this limitation is to introduce efficient pinning centers into crystals that can suppress the flux flow. A marked increase in J_c was observed in $Bi_2Sr_2CaCu_2O_{8+\delta}$ (Bi-2212) single crystals doped with a large amount of Pb. By electron microscopy, characteristic microstructures were revealed that probably underlie the observed enhancement in J_c: thin (10 to 50 nanometers), platelike domains having a modulation-free structure appeared with spacings of 50 to 100 nanometers along the *b* axis.

High-temperature copper oxide superconductors (HTSCs) exhibit an unusual magnetic field–temperature (*H-T*) phase diagram that differs from that of conventional superconductors (*1*, *2*). The major reason is the strongly two-dimensional (2D) character of HTSCs, as well as short coherence lengths and elevated critical temperatures (T_c's), which markedly change the vortex state in magnetic fields perpendicular to the CuO_2 layers; vortex lines become ill-defined and transform into pancake vortices confined within the CuO_2 layers, which couple only weakly between the layers (*3*). Consequently, the role of thermal fluctuation on the dynamics of vortices is enormously enhanced, and flux flow and flux-lattice melting occurs in a wide temperature range below T_c, resulting in a finite resistivity. A practically important boundary in the *H-T* phase diagram is called the irreversibility line (IL), which marks the boundary between the regions of reversible and irreversible magnetic behaviors (*2*). It is thought that the vortices are pinned by defects in crystals below the IL, whereas they can move in response to external forces above the IL, which means the vanishment of finite J_c (*4*). From the viewpoint of practical applications it is particularly important to expand this irreversible regime and, at the same time, to increase J_c.

Among the many HTSCs studied to date, Bi-2212 has been considered one of the most promising materials for use as wires for cables and magnets because of its chemical stability and flexibility in manufacturing processing: The melt-texture growth technique has sufficiently improved superconducting coupling between polycrystalline grains, which is another factor limiting the actual J_c value, and enabled the production of wires with relatively high J_c values below 20 K. However, one serious problem is that above 20 K J_c decreases drastically in magnetic fields (*5*). This decrease arises from the breakdown of the zero-resistive state due to thermally activated flux flow. Suppression of the flux flow is particularly significant for this compound because of its inherent 2D anisotropy (*6*). Large-scale applications would be accelerated by finding an appropriate solution to overcome this obstacle.

A key to increasing J_c is to generate efficient pinning centers in crystals (*7*). Recent studies with heavy-ion irradiation have demonstrated that aligned columnar defects serve as flux pinning centers and that the IL shifts upward (*8–13*). A similar improvement was recently reported for composites in which MgO nanorods 20 nm in diameter were embedded in matrix Bi-2212 films (*14*). We believe that an alternative method of generating efficient pinning centers in a more practical and useful way is necessary for future large-scale applications.

We investigated the single-crystal growth of Bi-2212 and found that the partial replacement of Bi with a large amount of Pb markedly affects the magnetic properties of Bi-2212. Pb substitution of about 0.3 per formula unit is essential to the formation of $Bi_2Sr_2Ca_2Cu_3O_{10+\delta}$ (Bi-2223) (*15*), whereas a range of solid solutions exists for Bi-2212 and $Bi_2Sr_2CuO_{6+\delta}$ (Bi-2201) (*16–18*). In the case of Bi-2212, single-phase materials were obtained for $0 \leq y \leq 0.8$ in a formula $Bi_{2-y}Pb_ySr_2CaCu_2O_{8+\delta}$ (*16*, *19*). Many single-crystal growth experiments have been carried out on pure Bi-2212 and Y-, La-, or Pb-doped systems (*20*, *21*). To our knowledge, however, there have been no attempts to prepare single crystals with amounts of Pb as large as $y > 0.4$.

Single crystals of Pb-substituted Bi-2212 were grown from starting compositions of $Bi_{2.2-x}Pb_xSr_{1.8}CaCu_2O_{8+\delta}$ (x = 0, 0.4, 0.6) by the conventional floating zone method with an infrared heating furnace. Crystals were grown in an atmosphere of 20% O_2–80% N_2, and the growth rate was 0.5 mm hours^{-1}. The composition of the grown crystals was examined by fluorescence x-ray com-

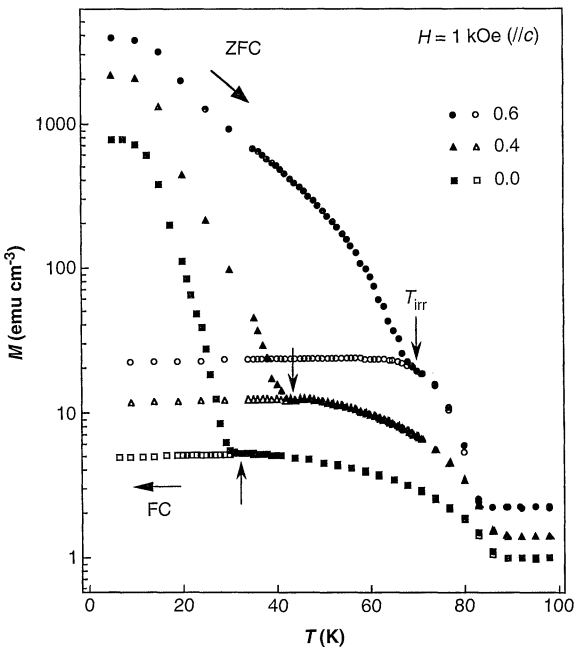

Fig. 1. Comparison of the temperature (T) dependence of magnetization (M) for the pure (x = 0) and the Pb-doped (x = 0.4 and 0.6) single crystals. Absolute values of M are displayed in a semilogarithmic plot. The data for x = 0.4 and 0.6 are multiplied by a factor of 2 and 4, respectively, for clarity. The measurements were carried out in a superconducting quantum interference device (SQUID) magnetometer ($MPMS_2$, Quantum Design) with a 4-cm scan length, with H approximately parallel to the *c* axis. In each measurement, the sample was rapidly cooled to 5 K in a nearly zero field, warmed slowly to 120 K in an applied field of 1 kOe (ZFC; filled symbols), and cooled again to 5 K (FC; open symbols). Magnetization of the sample holder, which was small (2×10^{-5} emu) and almost independent of temperature, was not subtracted.

I. Chong, Z. Hiroi, M. Izumi, T. Terashima, Y. Bando, M. Takano, Institute for Chemical Research, Kyoto University, Uji, Kyoto 611, Japan.
J. Shimoyama, Y. Nakayama, K. Kishio, Department of Applied Chemistry, University of Tokyo, Bunkyo-ku, Tokyo 113, Japan.
*To whom correspondence should be addressed.

position analysis. The results for $x = 0.4$ and 0.6 were $Bi_{1.86}Pb_{0.37}Sr_{2.11}Ca_{1.28}Cu_{2.00}O_{8+\delta}$ and $Bi_{1.84}Pb_{0.70}Sr_{2.19}Ca_{1.34}Cu_{2.00}O_{8+\delta}$, respectively, indicating little loss of particular elements. Platelike crystals of 1.0 by 1.0 by (~0.03 to 0.04) mm^3 were cleaved from each rod and used for magnetization measurements. A typical size of crystals used for resistivity measurements was 1.0 by 5.0 by 0.1 mm^3. Postannealing experiments were not done in the present study.

Magnetization measurements were carried out with H approximately parallel to the c axis of each crystal. Figure 1 compares the temperature dependence of magnetization for three crystals in an applied field of 1 kOe. The T_c onset—87, 85, and 83 K for $x = 0$, 0.4, and 0.6, respectively—was nearly equal for the three crystals. A large hysteresis was observed below the irreversible temperature T_{irr} at which the zero-field-cooled (ZFC) and the field-cooled (FC) branches coincided for each crystal. The most important feature was the drastic increase in T_{irr} with Pb content: 32 K ($x = 0$), 43 K ($x = 0.4$), and 70 K ($x = 0.6$). This result suggests that the Pb substitution suppresses flux flow at high temperature and leads to an increase in J_c, as occurs in ion-irradiated crystals with columnar defects (*8–13*).

The distinct improvement in J_c by Pb substitution was also detected in the resistivity measurements for $x = 0$ and 0.6 (Fig. 2). The tailing of the resistivity curve became more prominent with increasing magnetic field for the pure crystal, as reported previously, which is apparently due to the dissipation associated with flux flow (*22*). In contrast, the drop in resistivity remained much sharper even at $H = 1$ kOe for the Pb-doped crystal, indicating a large expansion of the temperature range with zero resistivity under magnetic fields.

Shifts of the IL toward values of high temperature and high magnetic field have important practical applications, because zero-resistive current can be transferred only below the IL in the H-T phase diagram. The ILs for the crystals in our study were determined by magnetization measurements as a function of temperature or field and are compared in Fig. 3. The IL shifted markedly upward with Pb doping. A drastic expansion of the irreversible regime was seen for $x = 0.6$, suggesting a substantial difference between the pinning mechanism of the $x = 0.6$ crystal and that of the others. The IL of the $x = 0.6$ crystal is comparable with those reported for heavy ion–irradiated single crystals (*13*) and the MgO nanorod composites (*14*).

We estimated the field dependence of J_c through magnetic measurements at fixed temperatures using the Bean model (*23*); in this model the hysteresis in magnetization, ΔM, is related to J_c as $J_c = 15\Delta M/r$, where r is the radius of the circulating current and is now assumed to be the lateral dimension of the crystal. Figure 4 presents the results for $T = 20$ and 30 K. A parallel upward shift with Pb content was seen in the J_c-H curves at 20 K. The absolute value for the pure crystal was nearly equal to those reported previously (*10*). At 30 K, in contrast, J_c fell rapidly with increasing field for $x = 0$, but Pb substitution up to $x = 0.6$ decreased the drop, maintaining J_c well above 10^4 A/cm^2 up to $H = 10$ kOe. These results demonstrated that very efficient pinning centers, which must be associated with the heavy Pb substitution, were introduced into the Bi-2212 crystals.

To clarify the pinning centers, we examined the microstructures of the three crystals by transmission electron microscopy. We prepared specimens for observation by crushing a crystal from the same batch used for magnetic measurements. Ten to 20 thin fragments were examined in a microscope for each specimen. Bi compounds exhibit a unique one-dimensionally modulated structure along the b axis that causes large, wavy displacements of atomic positions (*24*). The periodicity is $4.8b$ for pure materials, but increases with Pb doping; periodicities of $\sim 6.0b$ to $7.3b$ were reported for $y \approx 0.2$ to 0.3 (*16*, *25*, *26*). Even the disappearance of any modulation was reported for $y \geq 0.6$ in polycrystalline samples of Bi-2212 (*16*, *19*).

Electron diffraction experiments revealed that the modulation periodicity of the crystals changed systematically as $4.8b$ ($x = 0$), $\sim 7.0b$ to $7.3b$ (0.4), and $\sim 10.0b$ to $11.0b$ (0.6). Scattering in the periodicity from fragment to fragment was quite small. These results confirm that Pb was incorporated homogeneously in our crystals as ex-

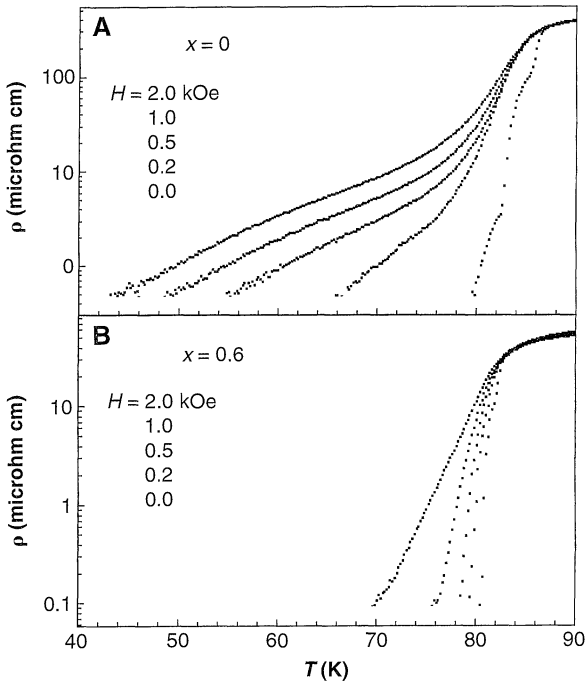

Fig. 2. Comparison of the evolution of resistivity curves in various applied fields for $x = 0$ (**A**) and 0.6 (**B**). The data were collected by the standard four-probe method with current passing along the c plane. The current density used was 4 A/cm^2. The magnetic field applied parallel to the c axis is increased from the right to the left as $H = 0$, 0.2, 0.5, 1, and 2 kOe. The multistep transition at $H = 0$ for $x = 0$ may be due to inhomogeneous distribution of oxygen in the crystal. Each crystal was not the same one used for magnetization measurements, but was taken from the same batch.

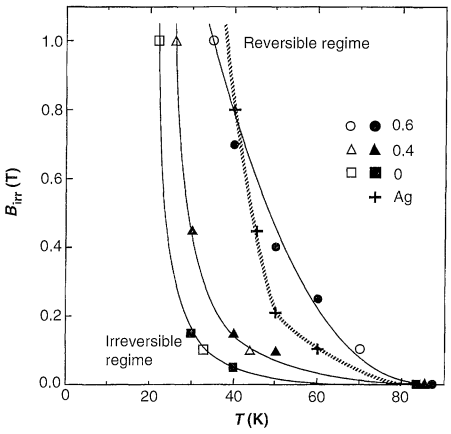

Fig. 3. Plots of the irreversibility field (B_{irr}) as a function of temperature for $x = 0$, 0.4, and 0.6. The data points shown with open symbols were determined by the measurements of M-T curves such as those in Fig. 1, whereas those with filled symbols were taken as the field at which hysteresis loops closed at each temperature. The solid line for $x = 0.6$ corresponds to a fit to $B_{irr} \propto (1 - T_{irr}/T_c)^n$ with $n = 2.2(2)$ (*36*). Such fitting was not successful for the data of $x = 0$ and 0.4. The solid lines for those data serve merely as guides to the eye. Also plotted for comparison is the B_{irr} of a Bi-2212 single crystal irradiated with 200-MeV Ag ions (*13*). The B_{irr} at $T > 40$ K is significantly larger in the Pb-doped crystal ($x = 0.6$) than in the heavy ion–irradiated one.

pected. Surprisingly, however, high-resolution electron microscopy (HREM) observations exhibited a distinct difference between the microstructures of the $x = 0.6$ crystal and those of the others. All the fragments with $x = 0$ and most with $x = 0.4$ were found to be homogeneous in the nanometer-scale range (*27*); a typical electron micrograph for $x = 0.4$ is shown in Fig. 5A. Regular modulation waves are apparent along the *b* axis over the entire particle.

In contrast, all the fragments with $x = 0.6$ exhibited an unusual microstructure. Bright horizontal stripes about 10 nm thick were apparent (Fig. 5B). They usually continued from one side of the particle to the other side but sometimes terminated within the particle. The spacing between two adjacent stripes was typically 50 to 100 nm. Their density varied slightly from fragment to fragment, but the stripes were always present. These domains probably have a thin, platelike shape aligned edge-on, because the diffraction contrast was very strong and the boundary with the matrix was sharp (*28*). Under magnification (Fig. 5C), a thin, platelike domain 8 nm thick was seen embedded in the matrix. Long-period fringes arising from the "normal" modulation were visible in the matrix, but such a superstructure was not discernible within the central domain. This finding implies a modulation-free structure or a long periodicity of >8 nm. However, we observed no modulation waves even in thicker domains (up to 50 nm) in other particles examined, which strongly suggests that the domains are essentially modulation free. Thus, the specific microstructure is probably due to a spatial variation in Pb content, because the modulation is expected to disappear for $2Pb/(Bi + Pb) > 0.6$ as reported in powder samples (*19*). This critical composition is close to the one we observed in the $x = 0.6$ crystal. It is likely that the solubility limit of Pb is higher in the melt or in the solid at high temperature and therefore that Pb-rich, modulation-free domains segregate in crystals at low temperature. This is not expected to occur in the crystals with starting Pb content lower than the solubility limit (for example, $x = 0.4$). A regular dislocation network such as that reported by Yang *et al.* (*29*) was not observed in any of our crystals.

The improvement in J_c and the upward shift of the IL in the heavily Pb-doped Bi-2212 single crystals could be due to the reduction of anisotropy, which would make the interlayer coupling stronger and stabilize a rigid flux-line lattice, or the introduction of effective pinning centers. Previously, a 20% Pb–substituted single crystal annealed in O_2 was characterized by a reduction in T_c to 70 K and by a reduction of 2D anisotropy compared with a pure crystal (*30*). These changes were attributed to overdoping of hole carriers (*31*). In contrast, the hole-doping level of the as-grown crystals used in our study seems to be close to the optimum level, judging from their high T_c's. Therefore, the reduction of the anisotropy by overdoping must be a secondary contribution in our study. This effect could account for the relatively small change observed in the IL from $x = 0$ to 0.4. We thus believe that the appearance of appropriate pinning centers needs to be taken into account.

The specific domain structure found by HREM only for the $x = 0.6$ crystal is suggestive of further research (*32*). The optimized T_c changes slightly with Pb doping; T_c first increases, reaches a maximum of 93 K at $y = 0.2$ or 95 K at $y = 0.4$, and then decreases to 90 K at $y = 0.6$ (*16*, *25*). In addition, the present Pb-substituted as-grown crystals lie in the anisotropy-reduced overdoped regime, and so T_c can be optimized by postannealing in a reducing atmosphere (*33*). Then, if the thin, platelike domains shown in Fig. 5 are richer in Pb content than the matrix (*34*), they would have a slightly lower T_c and a smaller anisotropy than the matrix. Moreover, the electron scattering at the boundaries may reduce the coherence length locally. These inhomogeneities may disturb flux flow and increase J_c. Such a correlated defect must suppress the thermal fluctuation of pancake vortices more efficiently than randomly distributed point defects (*35*).

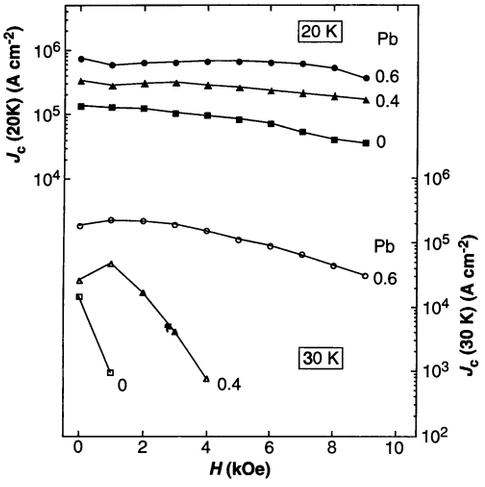

Fig. 4 (above). Comparison of the field dependence of J_c for the three crystals at 20 K (solid symbols) and 30 K (open symbols). The J_c's were determined from *M-H* hysteresis loops measured in a SQUID magnetometer with the Bean model.

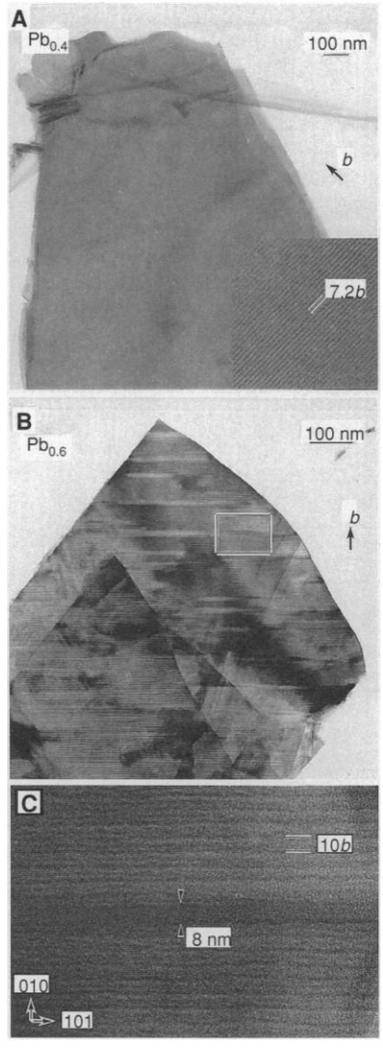

Fig. 5 (right). Electron micrographs showing microstructures of typical fragments for $x = 0.4$ (**A**) and 0.6 (**B**). Observations were carried out in a transmission electron microscope (JEOL-2000EX) operated at 200 kV. We prepared specimens for observation by crushing a platelike crystal, dispersing the fragments in acetone, and collecting them on a porous carbon film supported by a copper grid. The incident electron beam was parallel to the [10$\bar{1}$] direction so that the *b* axis was perpendicular to the incident beam. The magnification was slightly larger in (B) than in (A). The inset to (A) is a five times enlargement of the part of the image. The wide-stripe contrast seen from the top right to the bottom center in (B) is a supporting carbon film. (**C**) An enlargement of the rectangle in (B). The thickness of the domain is 8 nm, and the periodicity of the modulation wave is about 10*b* (5.4 nm) in the matrix above and below the lamella domain.

REFERENCES AND NOTES

1. D. J. Bishop, P. L. Gammel, D. A. Huse, C. A. Murray, *Science* **255**, 165 (1992).
2. G. Blatter, M. V. Feigel'man, V. B. Geshkenbein, A. I. Larkin, V. M. Vinokur, *Rev. Mod. Phys.* **66**, 1125 (1994).
3. J. R. Clem, *Phys. Rev. B* **43**, 7837 (1991).
4. E. H. Brandt, *Phys. Rev. Lett.* **63**, 1106 (1989).
5. H. Kumakura, K. Togano, H. Maeda, J. Kase, T. Morimoto, *Appl. Phys. Lett.* **58**, 2830 (1991).
6. Y. Kotaka *et al.*, *Physica C* **235**, 1529 (1994).
7. Two types of pinning centers have been characterized: point disorders (for example, neutron- or elec-

tron irradiation–induced defects, impurities, or oxygen vacancies) and correlated defects (for example, twin boundaries or columnar defects generated by heavy-ion irradiation). The former is effective at low temperature, whereas the latter plays a crucial role at high temperature.
8. L. Civale *et al.*, *Phys. Rev. Lett.* **67**, 648 (1991).
9. M. Konczykowski *et al.*, *Phys. Rev. B* **44**, 7167 (1991).
10. J. R. Thompson *et al.*, *Appl. Phys. Lett.* **60**, 2306 (1992).
11. W. Gerhauser *et al.*, *Phys. Rev. Lett.* **68**, 879 (1992).
12. H. Kumakura *et al.*, *J. Appl. Phys.* **74**, 451 (1993).
13. A. K. Pradhan *et al.*, *Phys. Rev. B* **53**, 2269 (1996).
14. P. Yang and C. M. Lieber, *Science* **273**, 1836 (1996).
15. M. Takano *et al.*, *Jpn. J. Appl. Phys.* **27**, L1041 (1988).
16. N. Fukushima *et al.*, *Physica C* **159**, 777 (1989).
17. Y. Ikeda *et al.*, *ibid.* **165**, 189 (1989).
18. P. Majewski, S. Kaesche, H.-L. Su, F. Alginger, *ibid.* **221**, 295 (1994).
19. H. Ito, Y. Ikeda, Z. Hiroi, M. Takano, Y. Bando, *J. Jpn. Soc. Powder Powder Metallurgy* **38**, 171 (1991).
20. T. Mochiku, in *Bismuth-Based High-Temperature Superconductors* (Dekker, New York, 1996), p. 227–237.
21. P. Fournier, A. Kapitulnik, A. F. Marshall, *Physica C* **257**, 291 (1996).
22. P. L. Gammel, L. F. Schnemeyer, J. V. Waszczak, D. J. Bishop, *Phys. Rev. Lett.* **61**, 1666 (1988).
23. C. P. Bean, *Rev. Mod. Phys.* **36**, 31 (1964).
24. Y. Matsui, H. Maeda, Y. Tanaka, S. Horiuchi, *Jpn. J. Appl. Phys.* **27**, L361 (1988).
25. J. L. Tallon, R. G. Buckley, P. W. Gilberd, M. R. Presland, *Physica C* **158**, 247 (1989).
26. D. J. Werder, C. H. Chen, S. Jin, R. C. Sherwood, *J. Mater. Res.* **4**, 748 (1989).
27. For the $x = 0.4$ crystal, about 10 fragments were examined in a microscope, and only one fragment exhibited a microstructure similar to that found in the $x = 0.6$ crystal. However, the domains in the $x = 0.4$ crystal were much smaller along the *a* axis (a few tens of nanometers) and were connected to each other to form meandering strings around the *a* axis.
28. Recently, cross-sectional HREM observations with an incident beam parallel to the *a* axis were performed on the $x = 0.6$ crystal. The results indicated that the typical length of the modulation-free domains along the *c* axis is a few micrometers, which means that the domains have a thin, platelike shape.
29. G. Yang *et al.*, *Phys. Rev. B* **48**, 4054 (1993).
30. R. Kleiner and P. Müller, *ibid.* **49**, 1327 (1994).
31. The relation between anisotropy and hole doping has been studied systematically in various HTSCs [K. Kishio *et al.*, *Physica C* **235**, 2775 (1994)]. With increasing hole-carrier density the anisotropy decreases, and thus B_{irr} increases.
32. It would be important to measure the angular dependence of pinning forces, because the domains have an anisotropic shape within the basal plane. The largest flux pinning should occur when the applied magnetic field is perpendicular to the *b* axis.
33. J. Shimoyama *et al.*, in preparation.
34. Recently, we detected a significant difference in the Pb content by using analytical electron microscopy.
35. The situation may be similar to that in the twin boundary in $YBa_2Cu_3O_{7-\delta}$, where the coherence length may be reduced due to electron scattering.
36. K. Kadowaki, in *4th International Symposium on Superconductivity (ISS '91), Tokyo*, H. Hayakawa and N. Koshizuka, Eds. (Springer Verlag, Tokyo, 1991), pp. 395–400.
37. We thank Y. Matsuda (Hokkaido University) for reviewing the manuscript and Rigaku Industrial Corporation for help with the fluorescence x-ray composition analysis. Supported in part by CREST (Core Research for Evolutional Science and Technology) of Japan Science and Technology Corporation (JST) and by the Original Industrial Technology R&D Promotion Program from the New Energy and Industrial Technology Development Organization (NEDO) of Japan.

31 December 1996; accepted 10 March 1997

High-Power Infrared (8-Micrometer Wavelength) Superlattice Lasers

Gaetano Scamarcio,* Federico Capasso,† Carlo Sirtori,‡ Jerome Faist, Albert L. Hutchinson, Deborah L. Sivco, Alfred Y. Cho

A quantum-cascade long-wavelength infrared laser based on superlattice active regions has been demonstrated. In this source, electrons injected by tunneling emit photons corresponding to the energy gap (minigap) between two superlattice conduction bands (minibands). A distinctive design feature is the high oscillator strength of the optical transition. Pulsed operation at a wavelength of about 8 micrometers with peak powers ranging from ~0.80 watt at 80 kelvin to 0.2 watt at 200 kelvin has been demonstrated in a superlattice with 1-nanometer-thick AlInAs barriers and 4.3-nanometer-thick GaInAs quantum wells grown by molecular beam epitaxy. These results demonstrate the potential of strongly coupled superlattices as infrared laser materials for high-power sources in which the wavelength can be tailored by design.

Semiconductor superlattices consist of a periodic stack of nanometer-thick layers of two materials (quantum wells and barriers) (*1*). The period *d* of this artificial crystal is typically much larger (~5 nm) than the lattice constant of the bulk crystalline constituents (~0.5 nm). This superimposed potential splits the conduction and valence bands in a series of much narrower bands (typically tens to a few hundred millielectron volts wide in the strong tunnel-coupling regime) called minibands, which are separated by energy gaps ("minigaps") along the direction normal to the layers (*1*). For a given choice of materials, miniband and minigap widths can be engineered by suitable choice of the layer's thickness, which can be atomically controlled with the use of thin-film crystal growth techniques such as molecular beam epitaxy (MBE) (*2*).

Although quantum wells, characterized by discrete energy levels caused by quantum confinement, have found wide use in semiconductor lasers for optical communications and optical recording and in other optoelectronic applications (*3*), the use of superlattices in optical devices has been limited. In their pioneering paper (*1*), Esaki and Tsu proposed their use as sources of submillimeter-wavelength coherent radiation emitted by electrons oscillating in phase in a high electric field normal to the layers (Bloch oscillations). This emission was recently observed (*4*) but is intrinsically of low power, and the goal of realizing an electrically pumped Bloch oscillator remains elusive.

We report a coherent infrared (IR) source based on strongly coupled superlattices that demonstrates the potential of these materials for lasers in the technologically important mid-IR spectrum. Laser action has been achieved between minibands through unipolar (electron) injection by interminiband tunneling. In our structure (Fig. 1), the laser transition is between states at the bottom of the second conduction miniband and empty states near the top of the first miniband at a photon energy well below the energy band gap of the barrier and well materials. The wavelength is thus determined by the minigap and can be selected in a large region of the IR spectrum by changing the barrier and well thickness. In the present structure, the wavelength λ was selected at $\cong 8$ μm, with the use of an eight-period superlattice with 1-nm-thick $Al_{0.48}In_{0.52}As$ barriers and 4.3-nm-thick $Ga_{0.47}In_{0.53}As$ quantum wells (*5*).

A distinctive design feature of this laser is the high oscillator strength of the direct optical transition at the mini–Brillouin zone boundary of the superlattice (Fig. 1B). The oscillator strength of radiative transitions between the first two minibands of a superlattice strongly increases with wave vector k_z as the barrier thickness is decreased and is maximum at the zone boundary ($k_z = \pi/d$) (*6*). For example, in our superlattice the ratio of oscillator strengths at $k_z = \pi/d$ and $k_z = 0$ is ~60, largely because of the variation of the transition matrix element z_{21} across the mini–Brillouin zone. By appropriately tailoring the barrier and well thickness, we optimized the structure for maximum oscillator strength (*6*) $f_{21} = (2m_0/\hbar^2)\hbar\omega z_{21}^2 = 55.4$ at $k_z = \pi/d$—where m_0 is the free electron mass and

Bell Laboratories, Lucent Technologies, 700 Mountain Avenue, Murray Hill, NJ 07974, USA.

*Present address: Dipartimento di Fisica, Università di Bari, 70126 Bari, Italy. E-mail: scamarcio@ba.infn.it
†To whom correspondence should be addressed. E-mail: fc@bell-labs.com
‡Present address: LCR Thomson-CSF, Domaine de Corbeville, 91400 Orsay, France.